



Effect of homogenization heat treatment on the microstructure of AZ91 magnesium alloy at different temperatures and ageing times

Taoheed Olohunde Sadiq^{a,b}, Izman Sudin^{a,*}, Ahmed Alsakkaf^a, Jamaliah Idris^a, Nor Akmal Fadil^a

^a Faculty of Mechanical Engineering, Universiti Teknologi Malaysia, UTM, Skudai, 81310, Johor Bahru, Malaysia

^b Office of the Governor, Government House, Abere, Osun State, Nigeria

ARTICLE INFO

Keywords:

Black chromium coating
Electroplating
Solar thermal application

ABSTRACT

Magnesium (Mg) alloys are promising biodegradable implant materials. If successful, they do not require a second surgical operation for their removal. These alloys possessed microstructure, which contained alpha (α -Mg) phase, eutectic ($\alpha + \beta$) phase and intermetallic or beta (β -Mg₁₇Al₁₂) phase. The bio-corrosion rate of any intermetallic alloy is related to its β phase volume fraction (VF). However, this β phase contributes galvanic corrosion which hinders the clinical application of Mg alloys. Thus, this study is focused to reduce the VF of the β phase and select the appropriate temperature for Mg homogenization heat treatment (HHT). HHT was carried out on Mg AZ91 alloy samples by using a high-temperature rotary furnace at 350 °C for 10 h, 370 °C for 10 h, 390 °C for 5 h and 10h, 410 °C for 5 h and 10h and 430 °C for 5 and 10 h. The influence of varying temperature with time was investigated on the microstructure and microhardness of Mg AZ91 alloy by using a field emission scanning electron microscope equipped with an energy-dispersive spectroscopy and image Digimizer. The results revealed that the higher the HHT or the longer the homogenization heat dwelling time, the more the homogeneous distribution of the large β phase over the microstructure, hence containing little or without a β phase. The microhardness increased with an increase in temperature and ageing time with the peak hardness at 410 °C and 430 °C for 10 h.

Introduction

Unlike conventional metallic implant materials, biodegradable implant materials do not call for second surgical operations for their removal after the healing. They are decomposed via a chemical medium by natural effectors, they are absorbed and excreted by the body without a trace and substituted by natural tissue [11]. Moreso, the second surgical operations require additional cost, involve risk and disadvantages after surgery. In addition, permanent implants are associated with many demerits; chronic inflammatory local reaction, inability to adapt to growth, stress shielding and accumulation of metals in tissue and physical irritation [2]. Biodegradable metallic implant materials are considered as a better alternative due to their suitability in high load-bearing applications [22].

Mg alloys had received great attention due to their distinguishable potentiality in biomedical applications where temporary stents are demanded. They are employed as a substitute for bone replacement due

to their biodegradability, biocompatibility and similarity in mechanical properties with natural bone [5]. Being their based element, Mg plays an essential role in human body metabolism and serves as one of the dominant elements in the human body serum [21]. The human consumption of Mg daily is suggested not to be more than 400 mg; however, the excess in daily Mg intake is not dangerous because it is excreted through urine [14]. A review of an article on new advances in the area of Mg degradation had been provided, and the importance of these material impacts, anodization, surface treatment and coatings on the corrosion behaviour of high-purity Mg was discussed [1]. The most common ones in Mg alloys are aluminium and zinc series alloys. Among these aluminium-zinc alloys is Mg AZ91 alloy, which had received great attention in medical applications [5]. Fundamentally, AZ91 Mg alloy comprises α phase, which is a solid solution of aluminium and Mg, and β phase made up of an intermetallic compound containing Mg and aluminium [4]. The β phase in AZ91 Mg alloy was observed and the findings revealed that this phase could either serve as a corrosion

* Corresponding author.

E-mail addresses: adisaloohunde@yahoo.com (T.O. Sadiq), izman@utm.my (I. Sudin).

<https://doi.org/10.1016/j.jer.2023.100133>

Received 21 October 2022; Received in revised form 4 April 2023; Accepted 12 April 2023

Available online 3 July 2023

2307-1877/© 2023 Published by Elsevier B.V. on behalf of Kuwait University. This is an open access article under the CC BY-NC-ND license (<http://creativecommons.org/licenses/by-nc-nd/4.0/>).

hindrance or corrosion enhancer depending on its distribution [19]. The continuous and fine distribution of the β phase enhances the improvement of corrosion resistance, while the discontinuous and coarsened one aggravates the degradation rate of Mg alloy [19]. In addition, the microstructure of Mg alloys is very important in determining their corrosion resistance. The corrosion behaviour of intermetallic phases such as α phase and β phase provides the background to study the effect of the microstructural multi-phases of metallic alloys [8]. Non-uniform distribution of these intermetallic phases may lead to differences in the degradation and mechanical properties of AZ91 alloy [15]. A homogenous microstructure with little or without an intermetallic phase is useful for corrosion resistance [16]. Thus, among the several solutions to tackle the demerit in AZ91 Mg alloy is by carrying out a surface modification with aim of achieving homogenous distribution of the β phase. Heat treatment is a promising technique to produce a passive Mg matrix and to enhance the corrosion resistance of Mg alloys [6]. The degradation rate of AZ91 alloy can be altered by modifying its microstructure through suitable heat treatment procedures [7]. Therefore, HHT was carried out at different temperatures and ageing times to reduce the volume fraction of the β phase and choose the appropriate temperature for Mg AZ91 heat treatment.

Material preparation

The part was cut from as-received biodegradable magnesium grade AZ91 alloy of $560 \times 70 \times 70$ (mm) using a power hacksaw, which was furtherly cut into 5 pieces of dimension $70 \times 70 \times 5$ (mm). Thereafter, they were milled and cut using wire-cut computer numerical control (CNC) machine into the samples with dimensions 10 mm x 10 mm x 3 mm. All these-operation was carried out at our mechanical workshop and production laboratory at the School of Mechanical Engineering, Universiti Teknologi Malaysia. The samples were washed ultrasonically with acetone and deionized water for 30 min to remove dirt. Finally, the AZ91 specimens were cleaned thoroughly with deionized water and aired at a room temperature [12]. For the analysis, the as-received samples were mechanically ground by using 400–4000 grit SiC paper and polished using alumina until mirror-like was achieved followed by etching in 2% nital for 10 s Table 1 presents the chemical composition of this AZ91 alloy as-received from the supplier, which was correlated with the previous studies.

Homogenization heat treatment

The HHT was conducted on as-received AZ91 alloy samples by using a high-temperature rotary furnace at 350 °C for 10 h, 370 °C for 10 h, 390 °C for 5 h and 10h, 410 °C for 5 h and 10h and 430 °C for 5 and 10 h based on the phase diagram and recrystallization temperature for magnesium-based alloy. The procedure was repeated to obtain the best microstructures for the samples. Due to the lightness and reactivity of Mg, the heat-treated samples were then cooled in the furnace to avoid Mg oxide formation in the air and catching fire in water quenching. For the analysis, the homogenised samples were mechanically ground by using 400–4000 grit SiC paper and polished using alumina until mirror-like was achieved, followed by etching in 2% nital solution for 10 s. Vickers hardness for the as-received and homogenized samples was measured. The microstructure was studied using a field emission scanning electron microscope equipped with an energy-dispersive spectroscope. Thereafter, the VF of the intermetallic phase was measured by using Digimizer as the image analyser. The as-received and homogenized samples were characterized by using X-ray diffraction analysis

technique to assess their phase compositions. Based on Vickers hardness, XRD and microstructural analysis, the homogenized sample with optimum temperature and ageing time was obtained.

Microstructure of as-received AZ91

Figs. 1 and 2 present the optical microstructure of polished unetched and etched surfaces of as-received AZ91 alloy, respectively. The microstructural surface reflects micro-porosity as demonstrated in Fig. 1. The dark dots are identified in the optical micrograph, which resembles micro-pores. The existence of micro-porosity in as-received magnesium AZ91 alloy conforms with previous studies [19]. Labelling the microstructure is possible as α -Mg matrix and intermetallic β -phase due to the different hardness between β -phase and α -phase that initiates a disparity in polishing rates [9].

The identified microstructure of as-received Mg AZ91 alloy as shown treated with 2% nital etching solution is displayed in the optical micrograph in Fig. 2 and field emission scanning electron microscope (FESEM) micrograph in Fig. 3. They show $\alpha + \beta$ (Eutectic) phase, magnesium-enriched phase (α -Mg) and β (Mg₁₇Al₁₂) phase precipitations [9].

As presented in Fig. 2, the as-received AZ91 alloy revealed spherical inclusions and networks along the grain boundaries. Fig. 3 revealed some dark sections in the surrounding of the grain boundaries, which could be attributed to the etching solution. These sections are known as the eutectic alpha (α) phase containing aluminium content more than the primary α phase [19]. This network of eutectic combinations with higher aluminium (Al) content contributes to the corrosion resistance which retrains the advance of the corrosion attack [24]. The FESEM microstructural image also revealed large β phase particles and $\alpha + \beta$ micro components in a fine lamellar combination as presented in Fig. 3. This fine lamellar arrangement in $\alpha + \beta$ micro constituents show the outline like the eutectic α phase due to the discontinuous formation of the β phase. The associated large β -particles are interconnected with the fine lamellar micro-constituents to produce an interrelated system throughout the microstructure. Additionally, the remaining part of the microstructure confined large β -phase particles encircled by the fine lamellar micro-constituent as secluded units in the alpha-phase matrix.

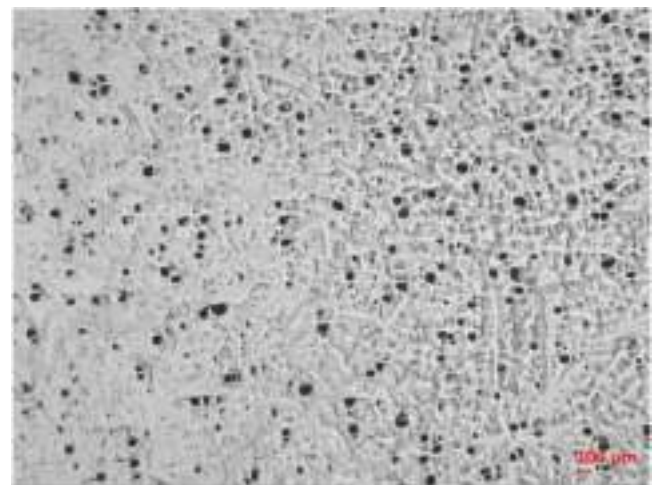


Fig. 1. Optical micrograph of unetched AZ91 alloy microstructure.

Table 1

The chemical composition of as-cast AZ91 alloy.

Element	Aluminium	Zinc	Manganese	Copper	Iron	Magnesium
% by weight	8.63	0.59	0.17	< 0.05	< 0.05	balance

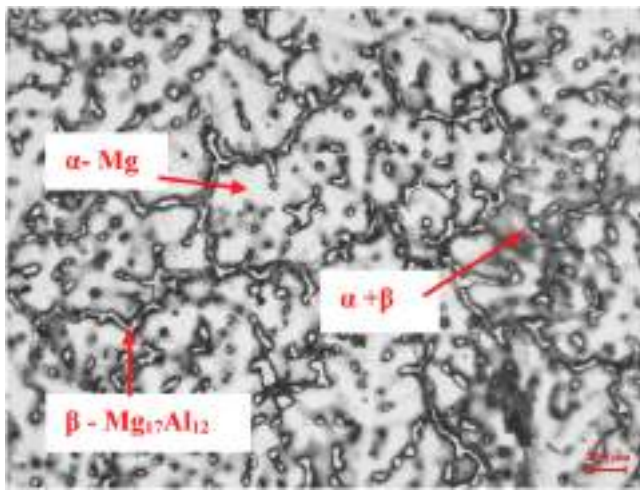


Fig. 2. Optical micrograph of etched AZ91 alloy microstructure.

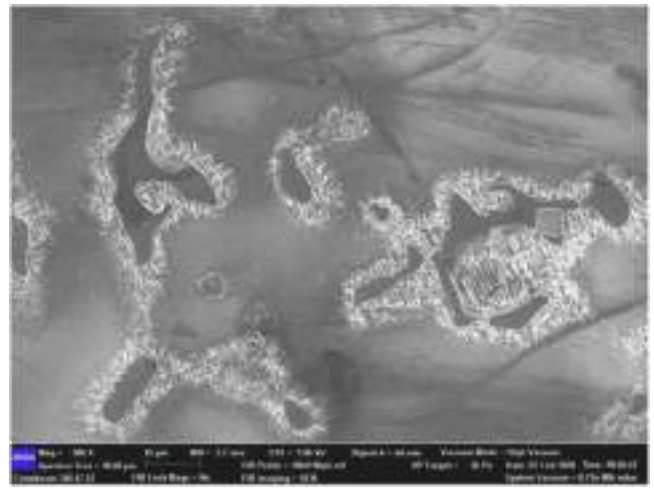


Fig. 4. FESEM image of AZ91 alloy after homogenization at 350 °C for 10 h.

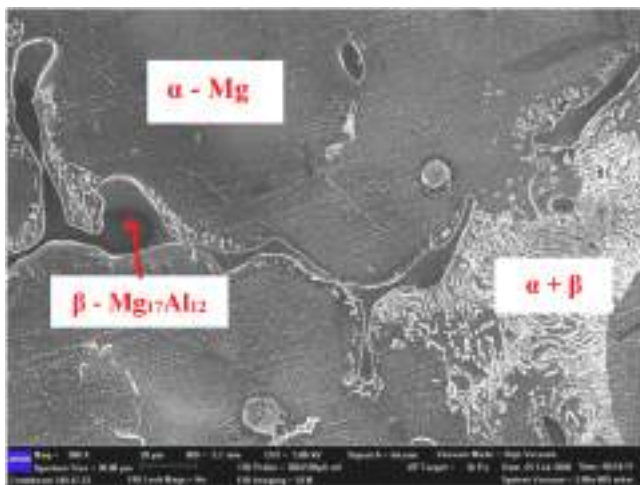


Fig. 3. FESEM image of as-received AZ91 alloy.

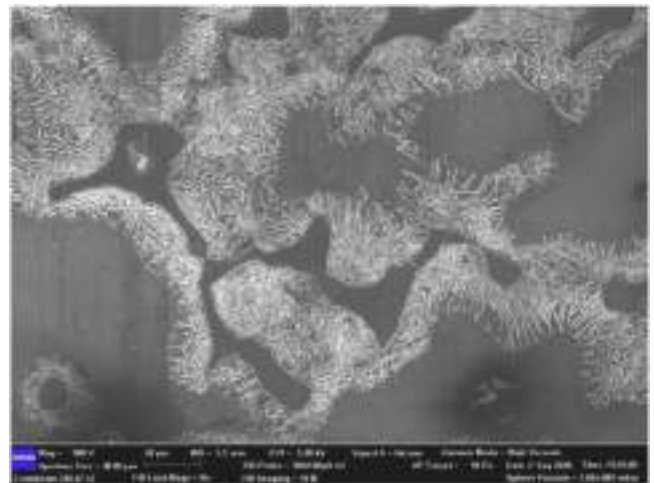


Fig. 5. FESEM image of AZ91 alloy after homogenization at 370 °C for 10 h.

Microstructure of AZ91 alloy after the heat treatment

There was a significant influence on the microstructure appearances of as-received AZ91 alloy after the HHT. Fig. 4 to Fig. 11 present a detailed comparison among the microstructures of different heat-treated AZ91 alloys. The VF of the β phase decreased considerably and distributed homogeneously with an increase in heat temperature or heat time. As shown in Fig. 4, after the HHT at 350 °C for 10 h, the β phase particles remained largely unaffected but most of the $\alpha + \beta$ (fine lamellar) micro constituents were almost dissolved. Nonetheless, the microstructure consistently consisted of the primary α matrix and un-detached large β phases accompanied by a small amount of the fine lamellar ($\alpha + \beta$) micro constituents appearing at the magnesium-enriched grain boundaries.

Fig. 5 presents the spectra after the HHT at 370 °C for 10 h. A large per cent of the fine lamellar micro constituents were almost dissolved with a noticeable decrease in the beta phases. There is consistency in the microstructure, containing α -Mg matrix, un-detached large β phases and a small volume of the fine lamellar micro constituents at the magnesium-enriched grain boundaries.

Figs. 6–7 present the spectra after the HHT at 390 °C for 5 h and 10 h respectively. The fine lamellar micro constituents dissolved completely,

and the β phase changed significantly. The microstructure also contained isolated particles and the primary alpha matrix. However, there was a greater reduction in the β phase after the HHT at 390 °C for 10 h as displayed in Fig. 7.

For the HHT at 410 °C/5 h as presented in Fig. 8, the fine lamellar micro constituents had been totally dissolved and beta phases had been largely dissolved. The FESEM spectrum showed a similar microstructure to what was obtained for the HHT at 390 °C for 10 h. However, the large β phase attained for the HHT at 410 °C for 5 h became smaller due to the part dissolution.

The microstructures of AZ91 alloy samples after HHT at 410 °C for 10 h and 430 °C for 5 h remain almost the same as presented in FESEM images; Fig. 9 and Fig. 10, respectively. The images showed that there is a change in the microstructure of as-received AZ91 alloy after the HHT. The large decrease in VF of β phase occurred due to prolonged annealing heat temperature and time, thereby causing β phase distribution to be more homogenous. Additionally, there was a large dissolution of fine lamellar constituents and most dissolution of large β particles. The remaining relatively little beta particles were homogeneously distributed throughout the matrix.

As presented in Fig. 11 for the HHT at 430 °C for 10 h, there was not much difference in the microstructure characteristics compared with the HHT at 410 °C for 10 h and 430 °C for 5 h, the fine lamellar micro constituents had been typically dissolved and beta phase had been mostly dissolved.

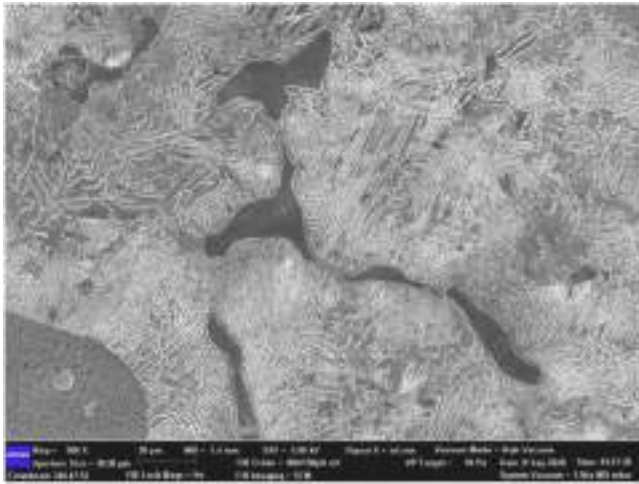


Fig. 6. FESEM image of AZ91 alloy after homogenization at 390 °C for 5 h.

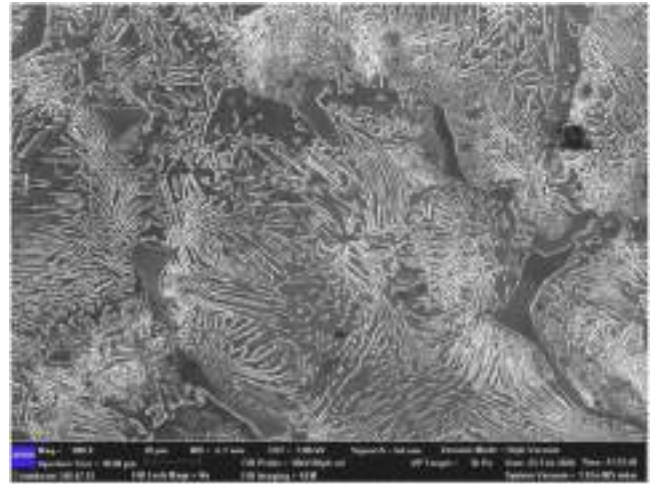


Fig. 9. FESEM image of AZ91 alloy after homogenization at 410 °C for 10.

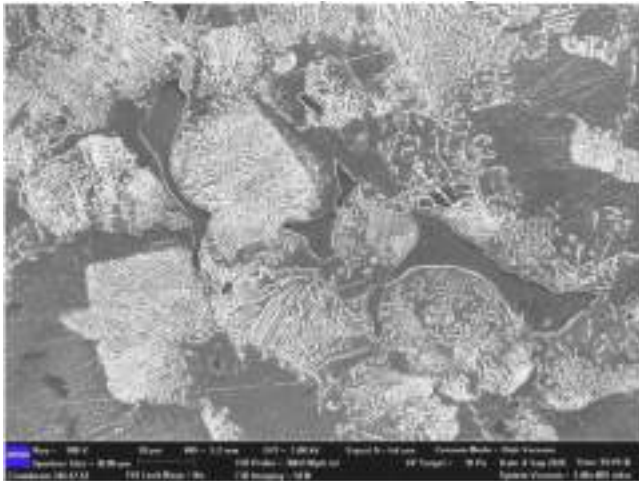


Fig. 7. FESEM image of AZ91 alloy after homogenization at 390 °C for 10 h.

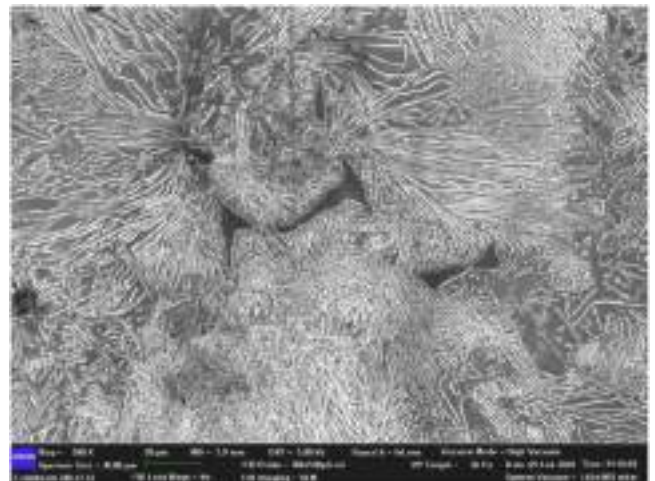


Fig. 10. FESEM image of AZ91 alloy after homogenization at 430 °C for 5 h.

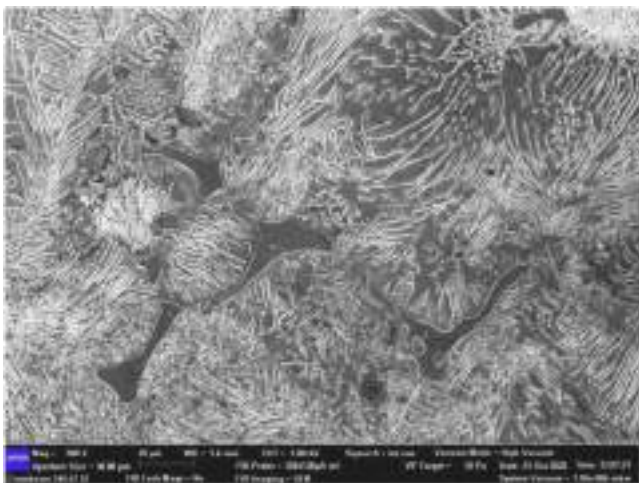


Fig. 8. FESEM image of AZ91 alloy after homogenization at 410 °C for 5 h.

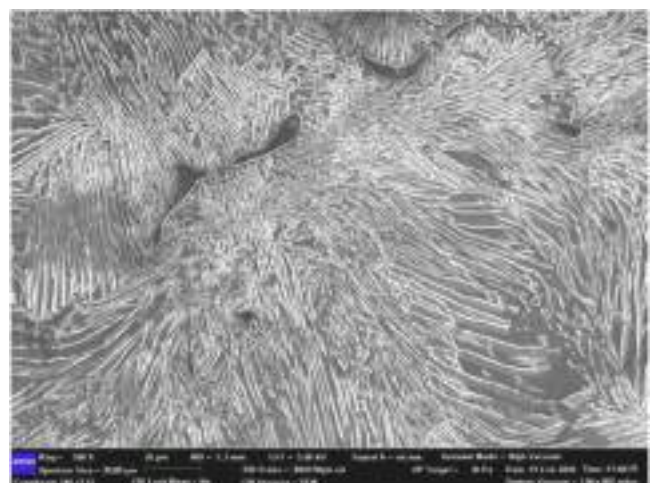


Fig. 11. FESEM image of AZ91 alloy after homogenization at 430 °C for 10 h.

Relatively, this left few beta particles distributed homogeneously over the matrix and a trace along the α phase grain boundaries of the $\alpha + \beta$ in the lamellar array.

Summarily, the HHT at 350 °C and 370 °C for 10 h induced little change to the large β phase and initiated mostly the dissolution of the fine lamellar ($\alpha + \beta$) micro constituents. However, there was a great

dissolution of the large β phase with the dissolution of the fine lamellar ($\alpha + \beta$) micro constituents for the HHT at 390 °C/5 h, 390 °C/10 h, 410 °C/5 h, 410 °C/10 h, 430 °C/5 h and 430 °C/10 h. Therefore, this shows that the higher HHT or the longer homogenization heat dwelling time yielded a more homogenous distribution of the large β phase over the microstructure.

Comparing the microstructures of AZ91 before and after the HHT, the form and VF of the second phase changed noticeably as presented in Fig. 3 – Fig. 11. The VF or amount of the β phase decreased dramatically, distributed along the grain boundaries, and inside the primary α matrix in form of small strips or particles. Generally, it is believed that homogenization heat treatment of AZ91 alloy contains a solid solution and precipitation of the intermetallic (second) phase [17,23]. Fig. 3 – Fig. 11 also presents the EDS area analysis for the as-received and different homogenization heat-treated AZ91 alloys. During the heat treatment, the aluminum solid solubility in the magnesium matrix increased due to the increase in temperature as the β -Mg₁₇Al₁₂ phase dissolved along the grain boundary in the primary alpha (α -Mg) matrix as presented, which in turn could enhance the mechanical properties of AZ91 alloys. In addition, as the homogenization heat temperature increased, the zinc content increased thereby, causing AZ91 alloy to be corrosion protective. However, as the AZ91 samples were subjected to HHT temperature, some of the elemental compositions i.e., copper, iron and magnesium disappeared.

VF of the as-received and homogenized AZ91 B phases

Table 2 presents the VF of the β phase of as-received and homogenized AZ91 alloys. The bio-corrosion rate of any intermetallic alloy is related to its secondary (intermetallic) phase VF [13]. The amount of the secondary phase is a key influencer in controlling the alloy corrosion rate [13]. A homogenous microstructure with little or without the secondary phase is helpful for the corrosion resistance [16]. The sample with a large VF of the secondary phase has the largest corrosion rate because the intermetallic phase causes galvanic corrosion, which limits the beneficial effect of fine grains [10]. The as-received AZ91 sample had the highest VF of the secondary phase while the lowest volume fraction was recorded in the high-temperature heat-treated AZ91 sample. A small VF of the secondary phase was achieved for the AZ91 sample heated at 410 °C temperature for 10 h and there was no significant difference after heating at a higher temperature.

Vickers hardness test

The Vickers hardness results of as-received and homogenized Mg alloy samples at 350 °C/10 h, 370 °C/10 h, 390 °C/5 h, 390 °C/10 h, 410 °C/5 h, 410 °C/10 h AZ91, 430 °C/5 h and 430 °C/10 h are presented in Table 3 and plotted in Fig. 12. The hardness of each sample increased with an increase in temperature and ageing time, with the peak hardness at 410 °C and 430 °C/10 h. This agreed with the previous study that the mechanical properties of the alloys are improved if the materials are slowly cooled inside the furnace [20]. The improvement

Table 3

The Vickers hardness (HV) test of AZ91 before and after HHT.

Stages	Average
As received	75
350 °C/10 h	81
370 °C/10 h	83
390 °C/5 h	86
390 °C/10 h	89
410 °C/5 h	90
410 °C/10 h	92
430 °C/5 h	92
430 °C/10 h	93

recorded showed that the AZ9 alloy possessed the required strength for the stated purpose.

XRD of AZ91 alloy before and after the heat treatment

Fig. 13 presents the XRD patterns of Mg AZ91 alloy specimens before and after the HHT. The microstructure of Mg AZ91 alloy contains magnesium-enriched matrix (α -Mg), $\alpha + \beta$ (Eutectic) and second or intermetallic β (Mg₁₇Al₁₂) phase precipitations as shown in Figs. 2 and 3 in conjunction with earlier studies [18]. These XRD spectra revealed β phase as(Mg₁₇Al₁₂) because all peaks in the XRD patterns matched to either the magnesium-enriched matrix (α -Mg) or β phase. Though, the previous study showed that the intermetallic β phase may appear as (Mg₄Al₃) (J, 1989; [3]). Thus, radiation diagrams confirmed that Mg AZ91 alloy contained magnesium-enriched matrix (α -Mg) and second/intermetallic β phase(Mg₁₇Al₁₂) before and after the HHT. The significant difference recorded in the comparative heights for the peaks associated with the magnesium-enriched matrix of as-received and heat-treated AZ91 alloy samples occurred because of microstructural changes due to the different homogenization heat temperatures and ageing times. The highest peak was recorded at a heat temperature of 410 °C for 10 h as the ageing time. There was a great reduction in peak height at higher heating temperatures and ageing times. This collaborated with the condition noticed for the microstructure analysis at these conditions. After the heat treatment, some of these phase compositions of the micro-constituent had largely disappeared, leaving a largely magnesium-enriched (α -Mg) phase. All the peaks were either from the magnesium-enriched matrix (α -Mg) or intermetallic (β -Mg₁₇Al₁₂) phase, marked with a circle.

Consequently, considering the Vickers hardness, XRD analysis and volume fraction (%) of the secondary phase for all the homogenized AZ91 samples at 350 °C/10 h, 370 °C/10 h, 390 °C/5 h, 390 °C/10 h, 410 °C/5 h, 410 °C/10 h, 430 °C/5 h and 430 °C/10 h, the homogenized AZ91 sample at 410 °C/10 h was obtained as the best sample.

Conclusion

The HHT at 350 °C and 370 °C/10 h effected little change to the large β phase and initiated mainly the dissolution of the fine lamellar ($\alpha + \beta$) micro constituents. However, the HHT at 390 °C/5 h, 390 °C/10 h, 410 °C/5 h, 410 °C/10 h, 430 °C/5 h and 430 °C/10 h effected great dissolution of the large β phase with the dissolution of the fine lamellar ($\alpha + \beta$) micro constituents. This revealed that the higher homogenization heat temperature or the longer homogenization heat dwelling time yielded a more homogenous distribution of the large β phase over the microstructure. In addition, the as-received AZ91 sample had the highest VF of β phase while the lowest VF was recorded in the high-temperature heat-treated AZ91 samples. A small VF of β phase was achieved for the AZ91 sample heated at 410 °C temperature for 10 h and there was no significant difference after heating at a higher temperature. The hardness of each sample increased with an increase in temperature and ageing time with the peak hardness at 410 °C and 430 °C for 10 h. A

Table 2

Intermetallic phase of AZ91 alloy before and after HHT.

Stage	VF (%) of AZ91 secondary phase
As-received	7.7
350 °C/10 h	7.4
370 °C/10 h	7.0
390 °C/5 h	6.0
390 °C/10 h	4.9
410 °C/5 h	3.5
410 °C/10 h	1.6
430 °C/5 h	1.4
430 °C/10 h	1.1

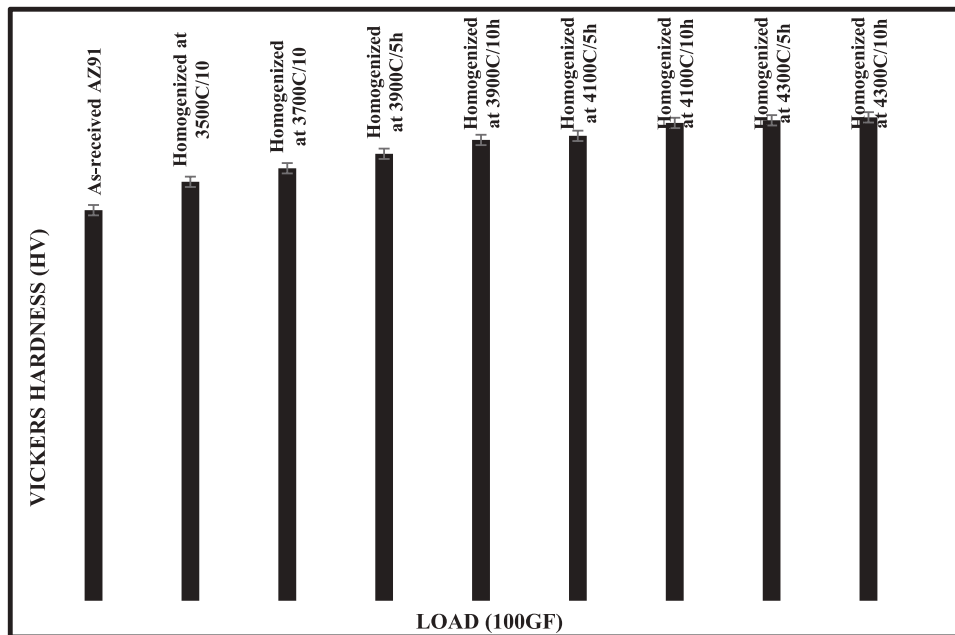


Fig. 12. Vickers microhardness test of as-received and homogenized AZ91 magnesium alloy samples.

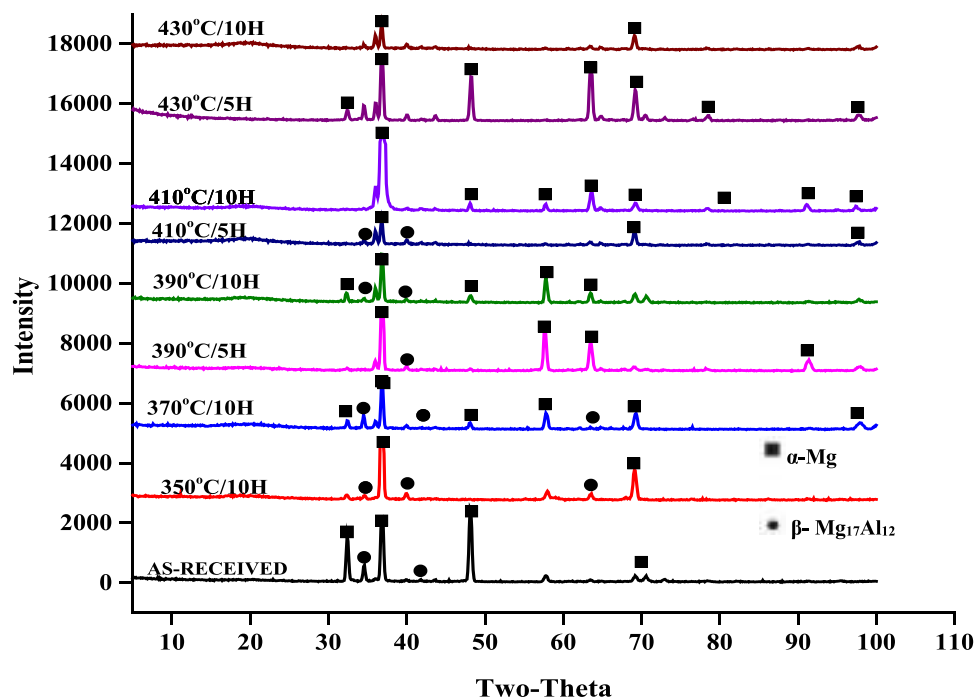


Fig. 13. XRD patterns of Mg AZ91 alloy specimens before and after the HHT.

significant difference in the comparative heights for the peaks associated with the magnesium-enriched matrix of as-received and heat-treated AZ91 alloy samples was noticed in the samples' microstructure due to the different homogenization heat temperatures and ageing times. The highest peak was recorded at a heat temperature of 410 °C for 10 h as the ageing time. There was a great reduction in peak height at higher heating temperatures and ageing times. Thus, the homogenized AZ91 sample at 410 °C/10 h was obtained as the best sample.

Funding

This work was supported by the Ministry of Higher Education

Malaysia (MOHE), Research Management Centre, Universiti Teknologi Malaysia for their financial support during and after this work through [GUP no: R.J130000.7651.4C309].

Declaration of Competing Interest

The authors declare the following financial interests/personal relationships which may be considered as potential competing interests: Sudin Izman reports financial support was provided by Universiti Teknologi Malaysia.

References

- [1] A. Atrens, G.L. Song, M. Liu, Z. Shi, F. Cao, M.S. Dargusch, Review of recent developments in the field of magnesium corrosion, *Adv. Eng. Mater.* 17 (4) (2015) 400–453.
- [2] H.R. Bakhsheshi-Rad, E. Hamzah, M. Daroonparvar, R. Ebrahimi-Kahrizangi, M. Medraj, In-vitro corrosion inhibition mechanism of fluorine-doped hydroxyapatite and brushite coated Mg–Ca alloys for biomedical applications, *Ceram. Int.* 40 (6) (2014) 7971–7982.
- [3] Beck, A.V., 1943. *The technology of magnesium and its alloys*. FA Hughes & Company Limited.
- [4] B.M. Bharathi, R.V. Vignesh, R. Padmanaban, M. Govindaraju, Effect of friction stir processing and heat treatment on the corrosion properties of AZ31 alloy, *Aust. J. Mech. Eng.* (2020) 1–10.
- [5] A.I. Bitu, G.E. Stan, M. Niculescu, I. Ciuca, E. Vasile, I. Antoniac, Adhesion evaluation of different bioceramic coatings on Mg–Ca alloys for biomedical applications, *J. Adhes. Sci. Technol.* 30 (18) (2016) 1968–1983.
- [6] F. Cao, G.L. Song, A. Atrens, Corrosion and passivation of magnesium alloys, *Corros. Sci.* 111 (2016) 835–845.
- [7] N.M. Chelliah, P. Padaikathan, R. Kumar, Evaluation of electrochemical impedance and biocorrosion characteristics of as-cast and T4 heat treated AZ91 Mg-alloys in Ringer's solution, *J. Magnes. Alloy.* 7 (1) (2019) 134–143.
- [8] M.S. Dambatta, S. Izman, D. Kurniawan, S. Farahany, B. Yahaya, H. Hermawan, Influence of thermal treatment on microstructure, mechanical and degradation properties of Zn–3Mg alloy as potential biodegradable implant material, *Mater. Des.* 85 (2015) 431–437.
- [9] G.R. Ebrahimi, A.R. Maldar, R. Ebrahimi, A. Davoodi, The effect of homogenization on microstructure and hot ductility behaviour of AZ91 magnesium alloy, *Kov. Mater.* 48 (2010) 277–284.
- [10] M. Echeverry-Rendon, J.P. Allain, S.M. Robledo, F. Echeverria, M.C. Harmsen, Coatings for biodegradable magnesium-based supports for therapy of vascular disease: a general view, *Mater. Sci. Eng.: C.* 102 (2019) 150–163.
- [11] J. Han, P. Wan, Y. Sun, Z. Liu, X. Fan, L. Tan, K. Yang, Fabrication and evaluation of a bioactive Sr–Ca–P contained micro-arc oxidation coating on magnesium strontium alloy for bone repair application, *J. Mater. Sci. Technol.* 32 (3) (2016) 233–244.
- [12] N.S.M. Jaafar, T.O. Sadiq, J. Idris, T.G. Fadara, M.Z. Ahmad, A. Al bakoosh Abdelaalam, Z.H. Samsudin, Investigation of mechanical properties and microstructural analysis on palm oil chisel, *Mater. Today: Proc.* 46 (2021) 1582–1587.
- [13] Y. Lu, A.R. Bradshaw, Y.L. Chiu, I.P. Jones, Effects of secondary phase and grain size on the corrosion of biodegradable Mg–Zn–Ca alloys, *Mater. Sci. Eng.: C.* 48 (2015) 480–486.
- [14] A. Mochizuki, H. Kaneda, Study on the blood compatibility and biodegradation properties of magnesium alloys, *Mater. Sci. Eng.: C.* 47 (2015) 204–210.
- [15] W.C. Neil, M. Forsyth, P.C. Howlett, C.R. Hutchinson, B.R.W. Hinton, Corrosion of heat treated magnesium alloy ZE41, *Corros. Sci.* 53 (10) (2011) 3299–3308.
- [16] D. Orlov, K.D. Ralston, N. Birbilis, Y. Estrin, Enhanced corrosion resistance of Mg alloy ZK60 after processing by integrated extrusion and equal channel angular pressing, *Acta Mater.* 59 (15) (2011) 6176–6186.
- [17] R. Rojaee, M. Fathi, K. Raeissi, Controlling the degradation rate of AZ91 magnesium alloy via sol–gel derived nanostructured hydroxyapatite coating, *Mater. Sci. Eng.: C.* 33 (7) (2013) 3817–3825.
- [18] R. Rojaee, M. Fathi, K. Raeissi, M. Taherian, Electrophoretic deposition of bioactive glass nanopowders on magnesium based alloy for biomedical applications, *Ceram. Int.* 40 (6) (2014) 7879–7888.
- [19] G. Song, A. Atrens, M. Dargusch, Influence of microstructure on the corrosion of diecast AZ91D, *Corros. Sci.* 41 (2) (1998) 249–273.
- [20] T. Tański, L.A. Dobrzański, L. Čížek, Influence of heat treatment on structure and properties of the cast magnesium alloys, in: *Advanced Materials Research*, Vol. 15, Trans Tech Publications Ltd, 2007, pp. 491–496.
- [21] M. Tsang, A. Armutlulu, F. Herrault, R.H. Shafer, S.A.B. Allen, M.G. Allen, Development of electroplated magnesium microstructures for biodegradable devices and energy sources, *J. Micro Syst.* 23 (6) (2014) 1281–1289.
- [22] R. Ummethala, F. Despang, M. Gelinsky, B. Basu, In vitro corrosion and mineralization of novel Ti–Si–C alloy, *Electrochim. Acta* 56 (11) (2011) 3809–3820.
- [23] L. Zheng, H. Nie, W. Liang, H. Wang, Y. Wang, Effect of pre-homogenizing treatment on microstructure and mechanical properties of hot-rolled AZ91 magnesium alloys, *J. Magnes. Alloy.* 4 (2) (2016) 115–122.
- [24] W. Zhou, N.N. Aung, A. Choudhary, M. Kanouni, Evaluation of corrosion resistance of magnesium alloys in radiator coolants, *Corros. Eng., Sci. Technol.* 46 (4) (2011) 386–391.